t_{2g} versus all $3d$ localization in LaMO_3 perovskites (M=Ti–Cu): First-principles study

Igor Solovyev* and Noriaki Hamada
Joint Research Center for Atom Technology, Angstrom Technology Partnership, 1-1-4 Higashi, Tsukuba, Ibaraki 305, Japan

Kiyoyuki Terakura
Joint Research Center for Atom Technology, National Institute for Advanced Interdisciplinary Research, 1-1-4 Higashi, Tsukuba, Ibaraki 305, Japan

(Received 25 August 1995; revised manuscript received 10 November 1995)

Using the LDA+U method (where LDA is local-density approximation) we show that a separate treatment of t_{2g} and e_g electrons on transition-metal sites as localized and itinerant, respectively, gives an appropriate description for the band structure of LaMO_3 perovskites (M=Ti–Cu) and systematically improves results of the local-spin-density approximation (LSDA) for the ground-state and single-electron excited-state properties. The analysis is based on comparison with experimental magnetic, optical, and photoemission data. Parameters of the effective Coulomb interaction estimated for t_{2g} electrons and a role of e_g screening are discussed. The present approach accounts well for the insulating natures of $LaTiO_3$, $LaVO_3$, and $LaCoO_3$, for which the LSDA predicts metallic states. Changes of the LSDA band structure for $LaMnO_3$ and $LaNiO_3$ are almost negligible due to the very efficient screening of on-site t_{2g} interactions by e_g electrons.

I. INTRODUCTION

Transition-metal perovskites AMO_3 (A being the trivalent metal ion and M being the $3d$ transition metal) present a very interesting group of materials being possessed of an extremely rich variety of properties accompanying the metal-insulator transition which can be rather easily switched in both directions either by external factors such as temperature, magnetic field, or hydrostatic pressure or by doping effects. A renewed interest in these compounds is related mainly with the discovery of high T_c superconductivity in perovskite cuprates.[1] Very recently the $La_{1-x}D_xMnO_3$ oxides with D=Ca, Sr, Ba attracted considerable attention because of a huge negative magnetoresistance observed near room temperature[2,3] and temperature-dependent structural phase transition induced by an external magnetic field.[4]

The electronic structure of transition-metal perovskites has been studied on the base of two different schemes. One is the configuration interaction approach with model Hamiltonians applied to Anderson impurities and clusters.[5,6] These models can be very useful for understanding the underlying physics responsible for phenomena and provide many-electron solution of the problem by taking into account the multiplet splitting caused by on-site Coulomb and exchange interactions. At the same time this approach is essentially restricted by its applicability only to finite-size systems and completely disregards periodicity of correlated sites and dispersion of the bands in the solid. Also the model approaches suffer from quite a large number of adjustable parameters. Another possibility is to use the *ab initio* band-structure methods based on the local-spin-density approximation (LSDA). Very recently it has been shown that an application of this approach to LaMO_3 perovskites can be quite successful in describing their electronic structures for M=Cr–Cu both for the ground-state and single-electron excited-state properties[7–9] (note, however, that a small band gap for M=Co was not reproduced by LSDA). Details of the crystal structure distortions play a crucial role in reproducing the stable magnetic structure and the insulating state in this band picture. Nevertheless, many problems still remain unsolved in the standard LSDA technique. We just refer to some of them for LaMO_3 compounds. The LSDA fails to reproduce the insulating behavior for early transition-metal perovskites $LaTiO_3$ and $LaVO_3$ and systematically underestimate the energy band gap for other insulating compounds. The LSDA often underestimates the tendency toward magnetism for LaMO_3: calculated magnetic moments tend to be smaller than experimental ones, no magnetic solution has been found in the $LaTiO_3$ case, again in contradiction with experimental data.[10] Thus, the electron correlations in the LaMO_3 compounds are very important and should be considered more rigorously beyond the LSDA. The direct way to do it is to use the many-body perturbation theories and estimate the exchange-correlation self-energy (for example, in the commonly used GW approximation,[11]) but due to its complexity the application of this technique for real perovskite compounds is quite problematic. Only some empirical estimations for the self-energy have been done so far.[12] At the same time, more simplified methods can be used to improve the LSDA. One of them is to start from the uniform electron gas limit for exchange and correlations (corresponding to LSDA) and to include inhomogeneity effects through the generalized gradient approximation (GGA).[13] As is discussed elsewhere, we have found that GGA enhances the tendency towards orbital polarization in $LaVO_3$ and YVO_3 causing them to be insulating.[14] GGA enhances the crystal field splitting between t_{2g} and e_g states of $LaCoO_3$ making it also nearly insulating. Nevertheless, the band gap does not open quite well and moreover GGA improves the LSDA results for $LaTiO_3$ only partially.[15] Another possibility could be to accept an opposite (atomic) point of view on correlations between localized electrons and include them in the same form

as for the free-standing atom through renormalized parameters of electron-electron interaction which can be estimated in the framework LSDA (LDA+U method[16–18]). In this paper we investigate possibilities of the latter approach and perspectives of its applicability for the transition-metal perovskites. In Sec. II we present a brief review of the LDA+U formalism stressing the advantages of this description for localized electrons in comparison with the standard LSDA as well as some limitations peculiar to the method. In Sec. III we discuss results of the LDA+U calculations for LaMO$_3$ compounds assuming two points of view on localization for 3d electrons on the M sites, the standard view and the one proposed by us: in the former, all 3d electrons are supposed to be localized and influenced by the on-site Coulomb interaction screened by other (non-3d) electrons; in the latter, only 3d electrons of the t_{2g} character are considered as localized whereas the e_g ones are treated as itinerant in the scope of the standard LSDA approach and allowed to participate in the screening of on-site t_{2g} interactions. Such a separate treatment of t_{2g} and e_g electrons in transition-metal perovskites has a long history mainly associated with the so-called double-exchange interaction model widely used to explain the magnetic behavior of Mn-based compounds[19] without any serious analysis of its consequences on the electronic structure itself. In this paper we investigate the direct effects of such a separate treatment on the band structure and show that this is a quite appropriate description for the LaMO$_3$ perovskites. We demonstrate that all the problems of the LSDA mentioned above could be resolved by the LDA+U approach. Particularly, the Ti- and V-based perovskites exhibit insulating (Mott-Hubbard) behavior in this approach with $U_{\rm eff}\sim W$ ($U_{\rm eff}$ and W being the effective Coulomb interaction between t_{2g} electrons and t_{2g} bandwidth, respectively) in good agreement with experimental finding, thus revising the main drawback of the LSDA metallic picture for these compounds. In the rhombohedral paramagnetic LaCoO$_3$, the correction applied to t_{2g} states increases the energy separation between t_{2g} and e_g bands, which is sufficient for opening a small band gap. Finally, short conclusion remarks will be given in Sec. IV.

II. METHOD

We start with the spin-polarized generalization of the LDA+U method (so called LSDA+U; see, for example, Refs. 18 and 20) and consider the total energy functional in the form

$$E[\rho^{\uparrow,\downarrow},\{\varphi_m^{\uparrow,\downarrow}\}]=E_{\rm LSDA}[\rho^{\uparrow,\downarrow}]+E_{\rm HF}[\{\varphi_m^{\uparrow,\downarrow}\}]-E_{\rm dc}[n^{\uparrow,\downarrow}], \tag{1}$$

where $E_{\rm LSDA}$ is the LSDA part depending on the components of spin density $\rho^{\uparrow,\downarrow}$ of the whole system, $E_{\rm HF}$ is the energy of the Hartree-Fock interaction between localized electrons with the same spin on the same site

$$E_{\rm HF}[\{\varphi_m^{\uparrow,\downarrow}\}]=\frac{1}{2}(U-J)\sum_{m\neq m'}\{n_m^{\uparrow}n_{m'}^{\uparrow},+n_m^{\downarrow}n_{m'}^{\downarrow},\} \tag{2}$$

in the basis $\{\varphi_m^{\uparrow,\downarrow}\}$ corresponding to the diagonal representation for the density matrix. We neglect the m dependence of Coulomb (U) and exchange (J) parameters in Eq. (2). The "double-counting" term $E_{\rm dc}$ in Eq. (1) serves to remove a part of the LSDA total energy corresponding to the interaction between localized electrons. In the LDA+U approach, the E_{dc} is chosen to be similar to the Hartree-Fock interaction energy (2) but expressed in terms of "spin-density." Due to the lack of self-interaction in Eq. (2), this correspondence can be found only in some limiting cases. In the "strongly localized" limit where the single-particle populations n_m^{σ} are close to 0 or 1, an appropriate expression for $E_{\rm dc}$ is

$$E_{\rm dc}[n^{\uparrow,\downarrow}]=\frac{1}{2}(U-J)\{n^{\uparrow}(n^{\uparrow}-1)+n^{\downarrow}(n^{\downarrow}-1)\} \tag{3}$$

which is used throughout in this work.

In contrast to Eq. (2), the $E_{\rm dc}$ depends only on the total number of the localized electrons for every spin channel n^{σ} and all information about individual populations is completely lost in the density-functional adapted expression (3). The interaction between electrons with different spins $Un^{\uparrow}n^{\downarrow}$ can be also formally included in Eq. (2), but it depends only on spin-density variables and will be exactly canceled by the same term appearing in the corresponding double-counting energy. Thus, in the spin-polarized version of the LDA+U method the strength of correction required for localized states is defined only by renormalized Coulomb interaction between the localized electrons with *the same spin*: $U_{\rm eff}=U-J$.

Then, the potential acting on the localized orbital ($m\sigma$) can be expressed as

$$V_m^{\sigma}(\mathbf{r})=V_{\rm LSDA}^{\sigma}(\mathbf{r})+(\tfrac{1}{2}-n_m^{\sigma})U_{\rm eff}. \tag{4}$$

There are two factors in favor of the LDA+U description for localized states in comparison with the standard LSDA.[18]

(i) The discontinuity of one-electron potential for localized states known for an exact density functional, which is responsible for population imbalance among orbitals in the narrow bands and formation of the Mott-Hubbard gap, is restored in the LDA+U approach [Eq. (4)].

(ii) Calculations of the quasiparticle spectrum for strongly correlated materials starting from LSDA remain quite a challenging problem and require large computational resources for its rigorous solution.[21] An approximate solution of the problem can be done using the LDA+U approach. The argument is based on Slater's transition state formalism,[22] which instead of regular LSDA eigenvalues prescribes to use those with half-integer occupations at the middle of corresponding excitation $\varepsilon_{\rm LSDA}^{\uparrow}(n^{\uparrow}\pm 1/2,n^{\downarrow})$ (analogous expression for spin down, $\pm$ correspond to the electron affinity and ionization potential, respectively). Using Taylor's expansion near the ground state configuration $(n^{\uparrow},n^{\downarrow})$ and parametrization of $\varepsilon_{\rm LSDA}^{\uparrow}$ in terms of Coulomb and exchange interaction parameters[18,23] $U-J=\partial\varepsilon_{\rm LSDA}^{\uparrow}/\partial n^{\uparrow}$ (see also the Appendix), we have

$$\varepsilon_{\rm LSDA}^{\uparrow}\left(n^{\uparrow}\pm\frac{1}{2},n^{\downarrow}\right)\simeq\varepsilon_{\rm LSDA}^{\uparrow}(n^{\uparrow},n^{\downarrow})\pm\frac{1}{2}U_{\rm eff}. \tag{5}$$

The expression for $+(-)$ sign corresponds to eigenvalues in LDA+U for empty (occupied) states if the hybridization effects are neglected [$n_m^{\sigma}=0$ or 1 in Eq. (4)].

TABLE I. Crystal and magnetic structure for LaMO$_3$ perovskites. M,O,R, and T denote the monoclinic, orthorhombic, rhombohedral, and tetragonal structure, respectively. A, C, and G correspond to different types of antiferromagnetic ordering, and P denotes paramagnetic states.

	LaTiO$_3$	LaVO$_3$	LaCrO$_3$	LaMnO$_3$	LaFeO$_3$	LaCoO$_3$	LaNiO$_3$	LaCuO$_3$
Crystal structure	O	M	O	O	O	R	R	T
Magnetic structure	G	C	G	A	G	P	P	P

The main disadvantage of the LDA+U approach is that it does not give any nonempirical prescription for the choice of localized states and their spatial extension. In principle, the last terms in Eqs. (4) and (5) are expected to be zero for an extended state in an infinite system and therefore the normal LSDA solution can be considered as a limiting case of LDA+U [in a direct analogy with SIC-LSDA (Ref. 24)]. Nevertheless one can show[18] that any localized solution in LDA+U corresponds to a LSDA-constraint approach. Therefore, its energy will always be higher than that of regular (itinerant) LSDA due to the variational principle for the total energy in the LSDA.[25] Thus, the energy minimization procedure is not applicable to the search for localized orbitals extension in LDA+U. Normally the choice of particular localized orbitals in LDA+U is based only on physical intuition like $3d$ states in the late transition-metal oxides[16,17] or $4f$ in the rare-earth compounds[26] and their spatial extension is modeled by numerical basis functions in the linear muffin-tin orbital method (LMTO).[27] This choice is based on the fact that basis functions in the LMTO associated with a given site have a definite principal quantum number – angular momentum (nL) character within the atomic sphere at this site and rapidly decay in the real space (corresponding to the form of envelope functions[27]). Moreover, by choosing the nearly orthogonal LMTO representation the basis can be expressed in the orthogonal form in analogy with the Wannier functions.

III. RESULTS AND DISCUSSIONS

We have applied the LDA+U approach to LaMO$_3$ perovskites using two different schemes to include the effects of localization on the $M(3d)$ states corresponding to two physically different points of view on localization in the $M(3d)$ shell. The first one (LDA+U_1) is the standard LDA+U algorithm where all $M(3d)$ electrons are supposed to be localized and experience the on-site Coulomb interaction correction. In the second scheme (LDA+U_2) we assume that only $3d$ states of t_{2g} symmetry exhibit the tendency toward localization whereas the e_g ones can be considered as itinerant within the LSDA scheme. In the perovskite structure, the t_{2g} and e_g bandwidths are determined mainly by π- and σ-type hybridization with O($2p$) states (in this respect the situation is different from the rock-salt oxides, where also the direct interaction between nearest transition-metal sites along the cube-face diagonal gives an appreciable effect on the t_{2g} bandwidths and is responsible for the mixing between t_{2g} and e_g bands[28]). Typically, the magnitude of the ($dp\pi$)-transfer integral is almost half of the ($dp\sigma$) one.[29] This difference naturally causes us to treat t_{2g} and e_g electrons separately: localized and much slower t_{2g} electrons are screened by itinerant e_g ones, which can immediately follow fluctuations of t_{2g} charges.

All calculations were performed using the ASA-LMTO method in the nearly orthogonal representation[27] for experimentally observed crystalline and magnetic structures listed in Table I, all details of which can be found in Ref. 7 and references therein. The tetragonal structure reported recently[30] has been used for LaCuO$_3$. As the basis functions, $M(3d,4sp)$, La($5pd$,$6sp$), and O($2sp$,$3s$) orbitals have been used. The $6p$ and semicore $5p$ states of La were treated in different energy panels: the first panel included low-lying bands formed mainly by La($5p$) and O($2s$) states whereas the basis functions of $3s$ type were used on oxygen sites in the second panel. The $4f$ states of La show another example of the strong intra-atomic Coulomb correlations in the LaMO$_3$ compounds. In accordance with bremsstrahlung isochromat spectroscopy data[31] they are located at about 10 eV above the Fermi level (E_F). The LSDA underestimates this energy separation [only 1.5-4.0 eV when M varies from Ti until Cu (Ref. 7)] with no evident influence of La($4f$) states on magnetic and insulating properties.[9] In the present work we do not include the La($4f$) states in the valence basis set at all, leaving the effects of localization in the $4f$ shell for future study. Keeping in mind that the ASA is rather a crude approximation for compounds possessing distorted crystalline structure we have performed as a test several LSDA calculations changing the ratios between Wigner-Seitz (WS) spheres for nonequivalent sites (while the total volume remains unchanged and equal to the experimental one). The WS radii chosen from the charge neutrality condition inside the spheres give the band structures for LaMO$_3$ perovskites in very reasonable agreement with results of more precise FLAPW calculations.[7,9] The ASA properly accounts for the hybridization effects for LaMO$_3$ and the choice of the neutral WS spheres minimizes uncertainty in the electrostatic potential, introduced by ASA.

A. Parameters of Coulomb and exchange interaction

Parameters of the electron-electron interaction for the LaMO$_3$ perovskites estimated by assuming different models for localization of the $M(3d)$ electrons are shown in Fig. 1. These calculations have been performed in a supercell geometry in order to simulate the impurity site which can exchange electrons but cannot hybridize with the rest of the system. The ideal (cubic) perovskite structure is assumed. The Coulomb interaction parameters U for two charge states ($2+$ and $3+$) of transition metal ions can be calculated using the standard LSDA-constraint technique.[23,32,33] For M^{2+} ions results are very close to analogous estimations performed for rock-salt transition-metal oxides.[16] In the M^{3+} case the strength of the Coulomb interaction is signifi-

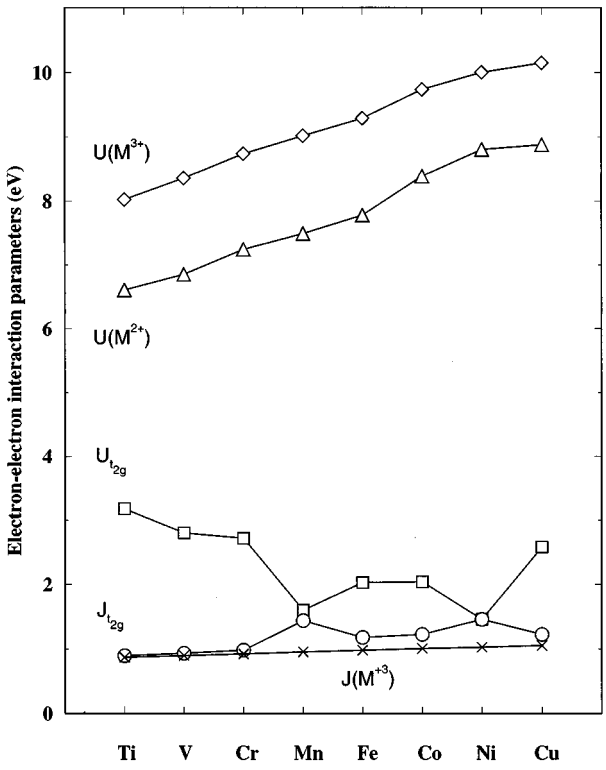

FIG. 1. Parameters of the electron-electron interaction for LaMO_3 calculated assuming trivalent (M^{3+}) and divalent (M^{2+}) configurations for transition-metal ions as well treating only t_{2g} states as localized.

cantly increased due to contraction of the $3d$ wave functions when the number of localized electrons decreases.[33] The static screening by an extra electron which has essentially long-range origin in the considered compounds (normally, only 25–30 % of the screening charge belongs to the same site) is not so efficient to reduce U for the M^{3+} configuration. Thus, decrease of effective Coulomb interaction in LaMO_3 perovskites in comparison with rock-salt oxides deduced from analysis of experimental photoemission data[29,31,34–36] cannot be explained by different static screening effects in M^{3+} and M^{2+} configurations. The third scheme used for an estimation of Coulomb and exchange parameters ($U_{t_{2g}}$ and $J_{t_{2g}}$ in Fig. 1) is based on an assumption that only $3d$ states of t_{2g} symmetry are localized whereas the e_g electrons are itinerant and allowed to participate in screening the localized t_{2g} electrons.[37] We have found the screening by e_g electrons to be very efficient and significantly reduces U for the t_{2g} shell. The exchange parameter J reveals an opposite tendency and slightly increases by e_g renormalization. Indeed, the effects of e_g screening are very different for U and J. Screened $U_{t_{2g}}$ is mainly defined by the term (see the Appendix)

$$U_{t_{2g}} \simeq \left(1+\frac{\delta n_{e_g}}{\delta n_{t_{2g}}}\right) U, \tag{6}$$

where U is the Coulomb interaction renormalized by other (non-$3d$) electrons. Due to the general tendency of local charge conservation $\delta n_{e_g}/\delta n_{t_{2g}} \leqslant 0$ and therefore $U_{t_{2g}} \leqslant U$. If the t_{2g} population is increased only at the expense of e_g electrons (and vice versa), $\delta n_{e_g} = -\delta n_{t_{2g}}$ and $U_{t_{2g}} = 0$.

Qualitatively, the reason for efficiency of the e_g screening is very simple. The renormalization of the Coulomb parameter by other interactions has a form $U = U^0 - U^0_{\rm scr}$, where U^0 is a bare interaction between localized electrons and $U^0_{\rm scr}$ is a screening interaction of localized electrons with the rest of the system. Normally, if the orbitals participating in the screening are spatially different from localized states (say $4sp$ and $3d$), $U^0_{\rm scr} < U^0$. Thus, this interaction cannot produce an absolute (100%) renormalization of the Coulomb U in principle. Even with a purely metallic mechanism when Coulomb interaction is screened entirely by the states belonging to the same site (which is believed to be the most efficient), U can be renormalized typically only up to ~ 4 eV for $3d$ sites.[23] When the nature of orbitals participating in screening is similar to the localized state, $U^0_{\rm scr} \sim U^0$ and the renormalization can be very efficient. Thus, the magnitude of the $U_{t_{2g}}$ parameter strongly depends on the nature of the states participating in renormalization: the more contribution from e_g orbitals, the more efficient screening.

Renormalization of the exchange interaction $J_{t_{2g}}$ is mainly given by

$$J_{t_{2g}} \simeq \left(1+\frac{\delta m_{e_g}}{\delta m_{t_{2g}}}\right) J. \tag{7}$$

The response of e_g states δm_{e_g} on small fluctuation of spin magnetization in t_{2g} states is governed by intra-atomic (Hund's) coupling which is always positive. Thus, $J_{t_{2g}} \geqslant J$.

Generally, the e_g screening is less efficient when the e_g states are either nearly empty or occupied, while it is enhanced at the half-filling case (Fig. 2). At the beginning of perovskite series M=Ti–Cr, $U_{t_{2g}}$ decreases slowly with increasing atomic number due to the systematical shift of the $M(3d)$ states to a lower energy region and partial population of the e_g states which screen the t_{2g} electrons more efficiently. Because of admixture into the O($2p$) band, the e_g population is typically 0.9, 1.0, and 1.1 for Ti, V, and Cr based compounds, respectively. Partial occupation of e_g band in $LaMnO_3$ significantly increases e_g population ($n_{e_g} \sim 2.1$) and drastically reduces $U_{t_{2g}}$ up to 1.6 eV. Subsequent population increase of e_g band in $LaFeO_3$ ($n_{e_g} \sim 3.0$) leads to somewhat poorer screening in comparison with the Mn case. The behavior of paramagnetic Co, Ni, and Cu perovskites having a fully occupied t^6_{2g} shell can be well understood again in terms of e_g band filling. For $LaCoO_3$ the situation is close to Ti, V, and Cr compounds with the unfilled e_g band except that in $LaCoO_3$ the empty e_g orbitals are located just above the Fermi level and screen the t_{2g} electrons more efficiently. In $LaNiO_3$ partial filling of the e_g band ($n_{e_g} \sim 2.4$) reduces the effective electron-electron interaction between t_{2g} electrons. The $LaCuO_3$ corresponds to the nearly occupied case ($n_{e_g} \sim 3.3$) and the e_g screening becomes again less efficient.

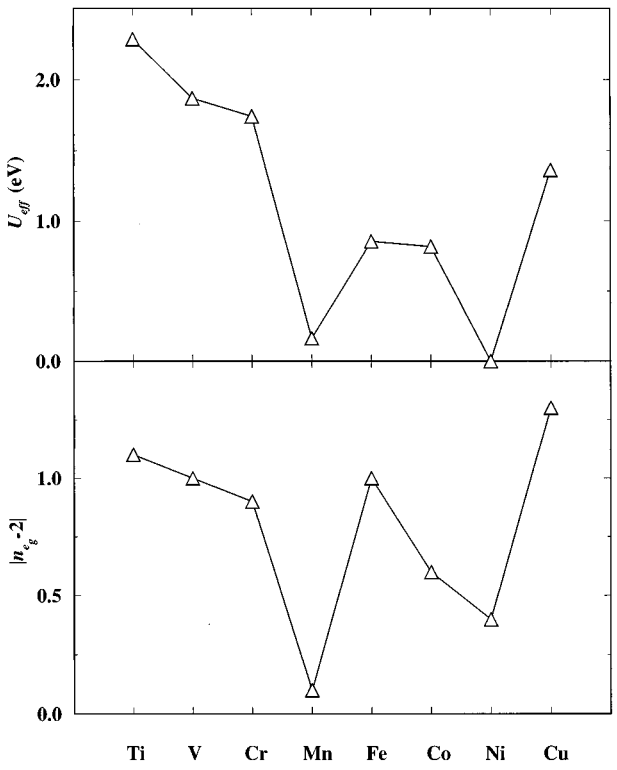

FIG. 2. Correlations between the strength of effective Coulomb interaction among t_{2g} electrons with the same spin $U_{\text{eff}} = U_{t_{2g}} - J_{t_{2g}}$ and the e_g population (n_{e_g}) at M site in LaMO$_3$ perovskites (Ref. 38).

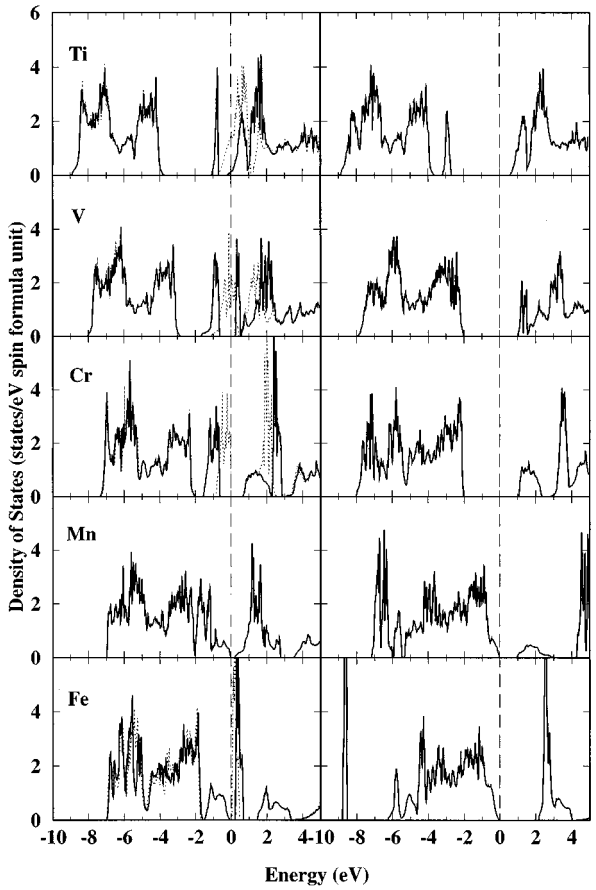

FIG. 3. Density of states for LaMO$_3$ perovskites with M=Ti–Fe obtained in LDA+U_1 (right panel) and LDA+U_2 (left panel) approaches. Dotted line corresponds to the LSDA. Position of the Fermi level is shown by vertical dashed line. The LDA+U_2 and LSDA curves were joined by the common O($2p$) band.

B. LDA+U and electronic structures of LaMO$_3$ perovskites

Having estimated parameters of the effective electron-electron interaction for the t_{2g} states we try to include them into the scheme for the band-structure calculations in the spirit of the LDA+U method. Strictly speaking distortions of the crystalline structure will lead to some mixing between $3d$ states of t_{2g} and e_g symmetries introducing some ambiguity in the choice of appropriate basis for localized states in the LDA+U_2 approach. We have performed two types of calculations for the LaMO$_3$ compounds with M=Ti–Fe crystallizing in the orthorhombic structure, where the crystal distortions are known to be much stronger than those in the rhombohedral one with M=Co,Ni, using slightly different orientations for the local coordinate system to estimate the local occupation numbers and to calculate corrections for the one electron potential [Eq. (4)]. In the first case, the orientation of the local system is chosen to be the same as that in the undistorted structure: $1/\sqrt{2}(1,\pm 1,0)$ and $(0,0,1)$ with reference to the **a**, **b**, and **c** directions in the orthorhombic cell. As another possibility we consider the local axis oriented to the nearest oxygen sites and somewhat tilted with respect to the previous choice. We have neglected small nonorthogonality in the latter local coordinate system. We have found that the results are very similar in both cases but the former choice, which we will consider in the following, gives systematically slightly lower estimations for the total energy.

Before showing results of LDA+U_2 calculations for early transition-metal perovskites M=Ti,V we would like to discuss briefly the qualitative aspect of the problem. The underlying physics responsible for the insulating behavior of considered compounds is based on the orbital instability effect[39] in the narrow t_{2g} band which appears at the Fermi energy in LSDA calculations (Fig. 3). In this respect the situation is very similar to FeO and CoO rock-salt oxides.[40] The bandwidth W is of the same order of magnitude as the effective Coulomb interaction between t_{2g} electrons with the same spin U_{eff}: W (U_{eff}) is 2.0 (2.3) and 1.5 (1.9) eV for Ti and V case, respectively. In a quantitative form the orbital instability criterion can be expressed as $N(E_F)U_{\text{eff}}>1$, where $N(E_F)$ is the density of states per spin and per orbital at the Fermi level. For real perovskites the situation is more complicated because the crystal distortions partially split the degenerate t_{2g} orbitals and this criterion becomes approximate. Nevertheless, such a splitting may be neglected in comparison with the t_{2g} bandwidth and the strength of the effective Coulomb interaction. Simple estimations give $N(E_F)U_{\text{eff}} = 1.1$ and 2.5 for Ti and V, respectively. Thus, the t_{2g} band will split by the on-site Coulomb interaction producing the insulating state in the early LaMO$_3$ perovskites.

Indeed, within the LDA+U_2 method both LaTiO$_3$ and LaVO$_3$ exhibit an insulating behavior. The t_{2g} states form three narrow bands around E_F (Fig. 3): the lower Hubbard (LHB) and two upper Hubbard (UHB) bands corresponding to different projections of spins. The second UHB overlaps

TABLE II. Energy band gaps (eV): fundamental (FG) and direct gaps (DG) in LSDA and LDA+U approaches and the experimental optical gap.

	$LaTiO_3$	$LaVO_3$	$LaCrO_3$	$LaMnO_3$	$LaFeO_3$	$LaCoO_3$
FG (LSDA)			0.6	0.1	0.1	
FG (LDA+U_1)	3.3	3.0	3.0	0.9	1.8	1.2
FG (LDA+U_2)	0.5	0.7	1.2	0.2	0.2	0.2
DG (LSDA)			0.6	0.7	0.1	0.1
DG (LDA+U_1)	3.5	3.2	3.0	1.4	1.8	1.2
DG (LDA+U_2)	0.8	0.9	1.2	0.7	0.2	0.2
Optical gap (Ref. 41)	0.1	1.1	3.4	1.1	2.1	0.3

with the e_g band, which starts around 1.5 eV. The energy separation between O($2p$) and the first UHB (charge transfer gap) is 4.5 and 3.5 eV for Ti and V perovskites, in good agreement with experimental optical data (4.5 and 4.0 eV, respectively[41]). Also the distance between O($2p$) and LHB (about 3 and 2 eV for Ti and V perovskites) is in good agreement with photoemission measurements.[12,31,42] The fundamental (minimum) and direct gaps are shown in Table II. For $LaVO_3$ agreement with experiment is fairly good, whereas for $LaTiO_3$ we failed to reproduce a sharp gap narrowing observed experimentally[41] (see also Ref. 42) which is attributed to many-electron effects in the unfilled t_{2g} band when $U_{\rm eff}\sim W$ (Ref. 12) and essentially beyond the one-electron description used in the present work (either in LSDA or LDA+U form). Nevertheless, we believe that LDA+U_2 scheme could be a good starting point for many-body applications in early transition-metal perovskites. On the contrary, LDA+U_1 considerably overestimates the splitting of t_{2g} states and the electronic structures of $LaTiO_3$ and $LaVO_3$ perovskites obtained in the scope of this scheme are rather far from realistic pictures: the band gap is much larger in comparison with the experimental one (Table II) and the relative position of O($2p$) and t_{2g} bands differs drastically from the one obtained in optical and photoemission measurements: for $LaTiO_3$, although LDA+U_1 reduces the band gap between the LHB and O($2p$) to a small value of $\sim$0.5 eV, it formally describes this compound still as a Mott-Hubbard insulator, whereas for $LaVO_3$ the occupied t_{2g} states fall into the O($2p$) band, making the band gap of the charge-transfer type (Fig. 3).

For LaMO$_3$ perovskites with M=Cr-Fe, even the standard LSDA reproduces the insulating state if the lattice distortions are taken into account properly. In the LDA+U_2 approach the M($3d$) states of t_{2g} symmetry split additionally by roughly $U_{\rm eff}$. In $LaCrO_3$ case with $U_{\rm eff}$=1.7 eV the effect is the most pronounced and considerably increases the energy gap formed by t_{2g} and e_g states with the same projection of spin (Fig. 3). For M=Mn due to very efficient screening by e_g states $U_{\rm eff}\sim$0 introducing almost negligible changes in the LDA+U_2 band structure in comparison with pure LSDA (Fig. 3). A similar situation occurs in $LaNiO_3$. The LSDA estimation for the transport gap in $LaMnO_3$ ($\sim$0.2 eV) is in very good agreement with resistivity measurements [0.24 eV (Ref. 3)], whereas the direct gap ($\sim$0.7 eV) between occupied and empty states in the same points of Brillouin zone (BZ) is underestimated in comparison with optical [1.1 eV (Ref. 41)] and photoemission [1.7 eV (Ref. 34)] data. In $LaFeO_3$ the $U_{\rm eff}$ shifts $t_{2g\downarrow}$ to the higher-energy region increasing the $e_{g\uparrow}-t_{2g\downarrow}$ separation (Fig. 3), but this effect is too small to reproduce the experimental energy gap (Table II). For paramagnetic rhombohedral $LaCoO_3$ (ionic configuration $t_{2g}^6e_g^0$) the $U_{\rm eff}$ pushes the occupied t_{2g} states to the lower energy region increasing separation between the t_{2g} and e_g bands which is sufficient to open a small energy gap (Fig. 4). The band-gap size estimated in LDA+U_2 as 0.2 eV is in good agreement with the experimental optical [0.2 eV (Ref. 41)] and resistivity [0.1 eV (Ref. 43)] data and somewhat smaller in comparison with photoemission measurements [0.6 eV (Ref. 35)]. In the least distorted $LaCuO_3$, the Cu(t_{2g}) states overlap with O($2p$) band and appreciably interact with the latter states. U_{eff} leads to some redistribution of the density of states within O($2p$) band with small influence on the behavior of $LaCuO_3$ in comparison with pure LSDA.

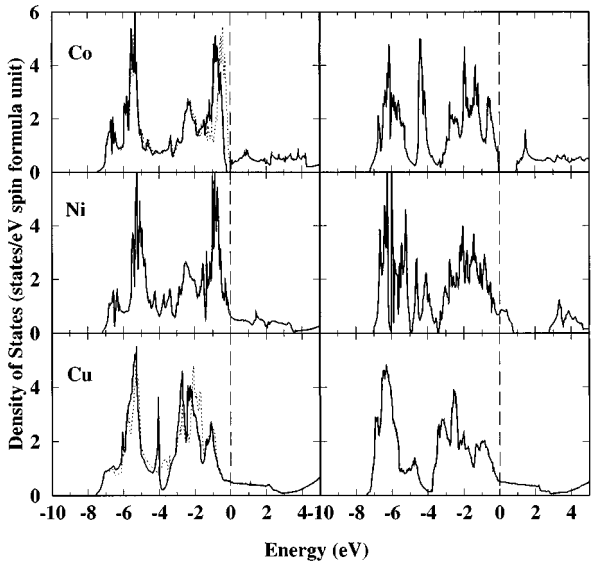

FIG. 4. Density of states for LaMO$_3$ perovskites with M=Co–Cu obtained in LDA+U_1 (right panel) and LDA+U_2 (left panel) approaches. Dotted line corresponds to the LSDA. Position of the Fermi level is shown by vertical dashed line. The LDA+U_1 result for $LaNiO_3$ corresponds to the antiferromagnetic configuration.

TABLE III. The local (spin) magnetic moments at the transition-metal sites (in μ_B). Two values for $LaVO_3$ correspond to nonequivalent V sites in the C-type antiferromagnetic state.

	$LaTiO_3$	$LaVO_3$	$LaCrO_3$	$LaMnO_3$	$LaFeO_3$
LSDA		1.85, 1.90	2.86	3.71	3.60
LDA+U_1	1.02	2.00, 2.00	3.18	4.20	4.04
LDA+U_2	0.92	1.98, 1.98	2.99	3.72	3.67
Experiment	0.45±0.05 (Ref. 10)	1.3±0.1 (Ref. 44)	2.8±0.2 (Ref. 45)	3.7±0.1 (Ref. 46)	4.6±0.2 (Ref. 45)

LDA+U_1 increases the band gap for Cr, Mn, and Fe perovskites in better agreement with the experimental optical photoemission data. We leave these discussions until the next sections where we will investigate the merits and demerits of different approaches based on the magnetic properties analysis and direct comparison with experimental optical spectra.

C. Magnetic properties

In Table III we show the (spin) magnetic moments at transition-metal sites obtained in the LSDA and different LDA+U approaches and compare them with experimental data. The LDA+U_2 systematically increases the local moments and yields the magnetic ground state in the $LaTiO_3$ case. Note that all magnetic solutions from ferro- to antiferromagnetic G type were found to be stable for the early transition-metal perovskites in the LDA+U_2 approach. For $LaCrO_3$ and $LaMnO_3$ agreement with experiment is remarkably good. The spin magnetic moments calculated for $LaTiO_3$ and $LaVO_3$ are larger than experimental magnetic moments. This tendency can be seen already in the LSDA for the $LaVO_3$ perovskite. We believe that the reason for these discrepancies is an unquenched orbital magnetization which can reduce the total magnetic moment on the Ti and V sites in accordance with Hund's third rule. In the ionic picture without crystal distortions the orbital magnetization induced by the spin-orbit interaction on the t_{2g} states is $1\mu_B$. The crystal distortions split the degenerate t_{2g} orbitals and partially quench the orbital moment. Thus, one can expect that the orbital magnetization will considerably improve the agreement with experiment for the $LaTiO_3$ and $LaVO_3$ compounds. As another possibility for discrepancies we could mention the canted magnetic structure which can arise also as a result of interplay between the crystal distortions and the spin-orbit interaction. We leave the effects of the spin-orbit interaction for future investigations. Importance of the spin-orbit interaction in Ti- and V-based perovskites has been also shown in Ref. 29 by using the periodical Anderson model. Calculated magnetic moments for $LaFeO_3$ are strongly underestimated in comparison with experimental ones. Even the LDA+U_1 scheme where all $3d$ states were supposed to be localized and feel a large Coulomb interaction gives only $4.04\mu_B$ for the local spin magnetization at the Fe site. The orbital magnetization is expected to be small for Fe atoms, which in this compound have an ionic configuration d^5, and cannot explain disagreement with experimental data. Indeed, the orbital magnetization estimated in LSDA for $LaFeO_3$ is only $0.05\mu_B$ per Fe site. For Ti-Mn compounds LDA+U_1 systematically overestimates the magnetic moments. Even if the discrepancies in Ti and V cases could be explained again by taking into consideration the orbital magnetization, this effect is expected to be very small for Cr- and Mn-based compounds having completely occupied $t_{2g}^{\uparrow}$ shell well separated from the states of e_g symmetry, because the energy separation considerably exceeds the strength of the spin-orbit interaction. The typical value of the orbital magnetization estimated for $LaCrO_3$ in LSDA is $-0.05\mu_B$ per Cr atom and the effect is even smaller for $LaMnO_3$. U additionally splits occupied $t_{2g}^{\uparrow}$ and empty e_g states and cannot increase the orbital moment in the $LaCrO_3$ case.

The magnetic behavior of the $LaMnO_3$ perovskite is particularly interesting, because in this e_g^1 system Jahn-Teller (JT) distortion is accompanied by the antiferromagnetic (A-type) spin and orbital ordering (alternately occupied $3x^2-r^2$ and $3y^2-r^2$ orbitals in the **ab** plane). Using the Green's-function technique, we have calculated parameters of the interatomic (Heisenberg's) exchange interaction[47]

$$J_{ij}=\frac{2}{\pi}\mathrm{Im}\int_{-\infty}^{E_F} dE\,\mathrm{Tr}_L\{G_{ij}^{\uparrow}(E)\Delta V_j G_{ji}^{\downarrow}(E)\Delta V_i\} \qquad (8)$$

for $LaMnO_3$ in LSDA and different LDA+U approaches. $G_{ij}^{\uparrow,\downarrow}$ in Eq. (8) is a block of real-space Green's function with the site indices ij; $\Delta V_i=V_i^{\uparrow}-V_i^{\downarrow}$, which can also depend on orbital indices due to the population imbalance in LDA+U or due to the effects of nonsphericity in the exchange potential in LSDA, Tr_L runs over the orbital indices. The first and second neighbor interaction parameters are listed in Table IV. LSDA and LDA+U_2 give very similar results for $LaMnO_3$ and we refer only to the former case. One can see that the behavior of t_{2g} and e_g contributions to the first neighbor exchanges is very different: the e_g-e_g interaction

TABLE IV. Parameters of interatomic exchange interactions between first (J^1) and second (J^2) Mn neighbors in $LaMnO_3$ calculated in LSDA and LDA+U_1 approaches (in kelvins). Two different values for J^2 correspond to nonequivalent pairs of second neighbors in the distorted orthorhombic structure.

	LSDA	LDA+U_1
	ab plane	
$J^1_{\mathbf{ab}}$ (total)	106	321
$J^1_{\mathbf{ab}}$ (t_{2g} only)	-107	-27
$J^1_{\mathbf{ab}}$ (e_g only)	261	350
$J^2_{\mathbf{ab}}$ (total)	-10,-27	1,0
	interplane	
$J^1_{\mathbf{c}}$ (total)	36	269
$J^1_{\mathbf{c}}$ (t_{2g} only)	-247	-66
$J^1_{\mathbf{c}}$ (e_g only)	271	310
$J^2_{\mathbf{c}}$ (total)	-33,-40	-19,-21

acts in favor of ferromagnetic arrangement between nearest Mn sites (both in and between **ab** planes), whereas $t_{2g}-t_{2g}$ exchange is essentially antiferromagnetic. In LSDA, the first neighbor interlayer $t_{2g}-t_{2g}$ and e_g-e_g interactions are of the same order of magnitude. Note that due to the tilted structure, a small mixed type $t_{2g}-e_g$ exchange also exists. The delicate balance between these two interactions depends on the strength of JT distortion and tilt of MnO_6 octahedra.[48] With the experimental crystal structure we found $J_{\mathbf{c}}^1$ to be weakly ferromagnetic and comparable with antiferromagnetic second neighbors exchange $J_{\mathbf{c}}^2$. Taking into account the coordination numbers, we have $2J_{\mathbf{c}}^1+8J_{\mathbf{c}}^2\simeq -220$ K. Thus, the LSDA could explain the A-type antiferromagnetism of $LaMnO_3$ associated with the JT distortion. Indeed, the total energy analysis[7–9] shows that the lowest energy in $LaMnO_3$ corresponds to the antiferromagnetic A-type arrangement. For weakly hybridized t_{2g} states, a larger spin splitting corresponds to a smaller interatomic exchange. In the LDA+U_1 approach, where the energy separation between spin up and spin down t_{2g} states is governed by large U (two peaks around -6.5 and 5 eV in Fig. 3), corresponding (antiferromagnetic) contributions to the first neighbor exchange are considerably reduced. The behavior of ferromagnetic e_g type exchange interactions is just the opposite: the potential term $\Delta V_i \Delta V_j$ in Eq. (8) is considerably larger in the LDA+U_1 approach, whereas the electronic structure factor related with the energy redistribution of e_g states is not directly affected by U due to the strong hybridization between $M(e_g)$ and O($2p$) states. Thus, LDA+U_1 overestimates the tendency toward ferromagnetism for the $LaMnO_3$ compound.

A gradual temperature-dependent transition between low- and high-spin states in $LaCoO_3$ was traditionally explained in the ionic picture, where the crystal field splitting between t_{2g} and e_g states is comparable with Hund's coupling.[36] LSDA, which shows a first-order transition between para- and ferromagnetic states in $LaCoO_3$ as a function of volume,[49] provides another point of view for this problem. This behavior is directly related with the shape of the density of states in this compound displaying a high t_{2g} peak and a broad e_g band near E_F in the paramagnetic phase (Fig. 4). Then, a magnetic solution becomes stable if

$$I\frac{2N^{\uparrow}(E_F)N^{\downarrow}(E_F)}{N^{\uparrow}(E_F)+N^{\downarrow}(E_F)}>1, \tag{9}$$

where I is Stoner's parameter, which can be calculated in the scope of LSDA,[50] and $N^{\uparrow,\downarrow}(E_F)$ is the density of states at the Fermi level split by a given initial magnetic field. When the splitting is vanishing $N^{\uparrow}(E_F)=N^{\downarrow}(E_F)=N(E_F)$, Eq. (9) is reduced to the standard Stoner criterion $IN(E_F)>1$ which is not fulfilled in $LaCoO_3$ having low density of states at the Fermi level in the paramagnetic phase. Thus, for a nearby experimental volume, the nonmagnetic solution is stable for $LaCoO_3$. If a field is strong enough, the conditions $N^{\uparrow}(E_F)\simeq N^{\uparrow}_{e_g}(E_F)$ and $N^{\downarrow}(E_F)\simeq N^{\downarrow}_{t_{2g}}(E_F)$ will be satisfied. Then, since $N^{\downarrow}_{t_{2g}}(E_F)\gg N^{\uparrow}_{e_g}(E_F)$, Eq. (9) is reduced to $2IN^{\uparrow}_{e_g}(E_F)>1$, which is the criterion for the high-spin solution in LSDA. For example, for the experimental volume this solution was found to be also stable with the spin magnetization of $1.3\mu_B$ per formula unit. The energy difference between these two states is very small in LSDA being comparable with kT. This feature could explain the temperature-dependent low-spin to high-spin transition in $LaCoO_3$. Two stable solutions for $LaCoO_3$ have been found also in the LDA+U_1 scheme: paramagnetic insulator having a configuration t_{2g}^6 and ferromagnetic half-metal having a t_{2g}^5 configuration with spin magnetization of $2\mu_b$ per formula unit. Nevertheless, the difference between these low-spin and high-spin solutions seems to be very overestimated: almost two orders of magnitude higher than kT.[51] In comparison with pure LSDA and the more traditional LDA+U_1, our LDA+U_2 approach provides an additional degree of freedom to explain the magnetic behavior of $LaCoO_3$, because in this compound magnetism is directly related with redistribution between t_{2g} and e_g populations. The strength of e_g screening is expected to be very different for different t_{2g} configurations (and therefore for different magnetic states). Indeed, the Coulomb interaction parameter U_{eff} estimated for t_{2g}^6, t_{2g}^5, and t_{2g}^4 configurations in $LaCoO_3$ is 0.8, 0.3, and 1.0 eV, respectively, again reflecting the degree of the filling of e_g states (nearly unoccupied, half-occupied, and completely occupied e_g shell). Thus, the t_{2g}^5 case is simply very close to the standard LSDA high-spin solution (also having t_{2g}^5 configuration). Here, we just wanted to illustrate some features of LDA+U_2 description of magnetic behavior of $LaCoO_3$ and leave more detailed analysis of this problem in future publications.

$LaNiO_3$ and $LaCuO_3$ show nonmagnetic behavior both in LSDA and LDA+U_2. On the contrary, both ferromagnetic and antiferromagnetic solutions with the spin moment $\sim 1.1\mu_B$ per M site have been found for $LaNiO_3$ in the LDA+U_1 approach, which due to the strong Coulomb correlations in unfilled e_g band overestimates the tendencies toward magnetism in this compound. Nevertheless, even in this approach $LaNiO_3$ remains metallic: E_F is located at the top of O($2p$) band and no band gap has been found (Fig. 4). Tetragonal $LaCuO_3$ is also metallic and shows a weak magnetism in the LDA+U_1: the magnetic moment at Cu site varies from $0.01\mu_b$ in ferromagnetic to $0.03\mu_b$ in the antiferromagnetic G-type configurations.[52] Finally, our results (both LSDA, LDA+U_1, and LDA+U_2) qualitatively agree with experimentally observed electric and magnetic properties of $LaCuO_3$ reported in Ref. 30: metallic behavior and possibly weak magnetism in the large U scheme. Nevertheless, our calculations do not support the point of view about the canted antiferromagnetic structure with large local magnetic moments at Cu sites proposed in Ref. 30. Evidently, more experimental information is needed to understand the behavior of $LaCuO_3$ compound.

D. Optical conductivity

In order to compare the band structures of the LaMO$_3$ perovskites obtained by different methods directly with experimental optical data we show in Fig. 5 the optical conductivity curves $\bar{\sigma}(\omega)=\frac{1}{3}\sum_{\alpha=1}^{3}\sigma_{\alpha\alpha}(\omega)$, where $\sigma_{\alpha\beta}$ is the conductivity tensor which generally includes two parts corresponding to interband and intraband transitions $\sigma_{\alpha\beta}=\sigma_{\alpha\beta}^{\mathrm{inter}}+\sigma_{\alpha\beta}^{\mathrm{intra}}$ (in Rydberg units):

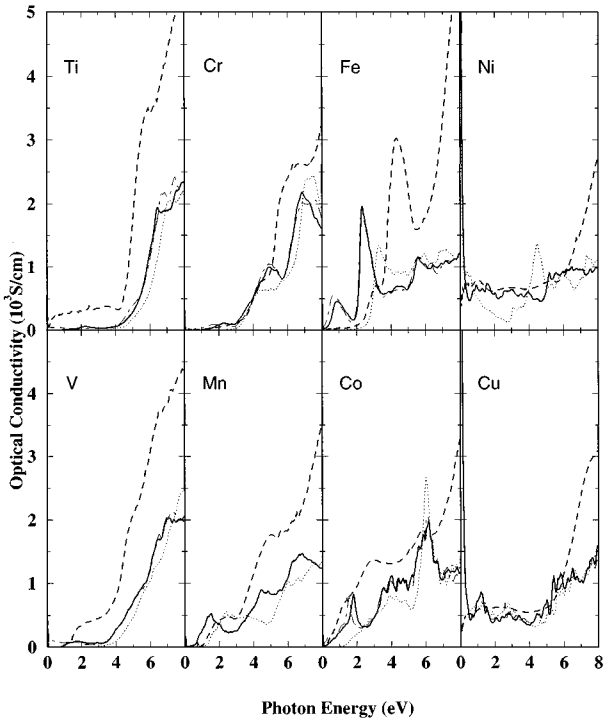

FIG. 5. Spectra of optical conductivity for LaMO$_3$ perovskites: LDA+U applied only for t_{2g} and for all 3d states (solid and dotted curves, respectively), LSDA (dot-dashed), experiment by Arima *et al.* (dashed). The LDA+U_1 result for LaNiO$_3$ corresponds to the antiferromagnetic configuration.

$$\sigma^{\text{inter}}_{\alpha\beta}(\omega)=\frac{1}{\pi^2}\sum_{\ell\neq\ell'}\int d^3\mathbf{k} f_{\ell\mathbf{k}}(1-f_{\ell'\mathbf{k}})\langle\ell\mathbf{k}|p_\alpha|\ell'\mathbf{k}\rangle \times\langle\ell'\mathbf{k}|p_\beta|\ell\mathbf{k}\rangle\frac{\delta(\omega-E_{\ell'\mathbf{k}}+E_{\ell\mathbf{k}})}{E_{\ell'\mathbf{k}}-E_{\ell\mathbf{k}}} \tag{10}$$

and

$$\sigma^{\text{intra}}_{\alpha\beta}(\omega)=\frac{1}{\pi^2}\delta(\omega)\sum_{\ell}\int d^3\mathbf{k}\langle\ell\mathbf{k}|p_\alpha|\ell\mathbf{k}\rangle \times\langle\ell\mathbf{k}|p_\beta|\ell\mathbf{k}\rangle\delta(E_{\ell\mathbf{k}}-E_F) \tag{11}$$

calculated in the random-phase approximation on the base of LMTO method.[53] $f_{\ell\mathbf{k}}$ is the zero-temperature Fermi distribution function for the state $|\ell\mathbf{k}\rangle$, p_α is the momentum operator $p_\alpha=-i\nabla_\alpha$, and the spin state index is included in the band index ℓ. The BZ integration has been performed in the uniform grid containing 2475 **k** points in the whole zone for perovskites with the orthorhombic structure of M=Ti–Fe (corresponding to 14 divisions along in-plane and 10 divisions along the perpendicular reciprocal-lattice vectors) and 3375 **k** points for the rhombohedral-phase compounds of M=Co,Ni (14 divisions along the reciprocal-lattice vectors). 6859 **k** points in the whole BZ (18 divisions along the reciprocal vectors) have been used for the tetragonal LaCuO$_3$. The intraband conductivity [Eq. (11)] has been calculated with the standard tetrahedron technique with correct weights for the tetrahedra. Using the method proposed in Ref. 54, the BZ integration in [Eq. (10)] has been replaced by the weighted sums in the analogy of the special-point scheme which considerably facilitates numerical calculations. Finally, we replaced the δ function in the BZ integral in Eq. (10) by Lorentzian: $\delta(\omega)\rightarrow\tau/[\pi(1+\omega^2\tau^2)]$ with the lifetime broadening τ^{-1}=5 mRy. The local field effects have been omitted.

For all compounds the LDA+U_2 approach well reproduces the main features of the optical spectra[41] in the low energy region. For LaTiO$_3$ and LaVO$_3$ the optical conductivity curves show a weak structure up to 4 eV corresponding to excitations from the t_{2g} LHB. Experimentally, this part of the spectra is more pronounced. We would like to comment here again that the spin-orbit interaction could significantly change the contents of the LHB and UHB (in favor of complex rather than real harmonics) and modify corresponding probabilities of optical transitions in Ti- and V-based compounds. The onset of the high intensity structure starting around 4 eV is formed mainly by transitions from the O $(2p)$ band to the t_{2g} UHB. In the higher energy region (around 5 eV) this structure is considerably enhanced by the O$(2p)$ to e_g excitations. The interband conductivity obtained in LSDA is very similar to that in the LDA+U_2 approach, because the probabilities of the optical transitions associated with $M(t_{2g})$ states are relatively small and the optical conductivity curve is rather insensitive to the position of the t_{2g} band. An intraband (Drude) peak appears in the optical conductivity curves in LSDA for early transition-metal perovskites M=Ti,V in obvious disagreement with experimental data. On the contrary, the LDA+U_1 scheme overestimates the band gap and in principle fails to reproduce the low intensity part of the spectra, spreading up to 4 eV.

For LaCrO$_3$ the low energy excitation (around 2.5 eV) in LDA+U_2 corresponds to the transition between occupied t_{2g} and unoccupied e_g bands (Fig. 3). The probability of this transition is much weaker than that of the next excitation from O$(2p)$ to e_g band (around 4 eV). It could be related with the low energy tail which is observed experimentally around 2.5 eV but disregarded in Ref. 41 due to its very low intensity. It could be also the reason for overestimation of the experimental optical gap in comparison with results of our LDA+U_2 calculations (Table II), because the optical gap was assumed in Ref. 41 as a charge-transfer gap between O $(2p)$ and e_g bands. In the LDA+U_1 approach the occupied t_{2g} states in LaCrO$_3$ appear at the bottom of the O$(2p)$ band (Fig. 3) making the insulating nature of LaCrO$_3$ in LDA+U_1 of the charge transfer rather than Mott-Hubbard type. On the other hand, the energy separation between O$(2p)$ and unoccupied e_g bands ($\sim$3 eV) is nearly the same in LSDA, LDA+U_1, and LDA+U_2 schemes. Thus, except the low intensity part around 2.5 eV, the optical spectra corresponding to these different methods are very similar and an analysis based only on optical data is not sufficient to distinguish between them. On the other hand, the x-ray photoemission spectra for LaCrO$_3$ (see Ref. 31 and references therein) show three-peak structure very similar to Ti and V perovskites. Thus, the low binding energy peak ($\sim$1.5 eV) can be identified with Cr(t_{2g}) states in favor of the Mott-Hubbard picture for the LaCrO$_3$ insulator.[31] This experimental fact is in line with LDA+U_2 rather than the LDA+U_1 approach. Moreover, the relative position of occupied Cr(t_{2g}) and O$(2p)$ bands obtained by LDA+U_2 fits well to the shape of the x-ray photoemission spectra.

The minimum optical gap in $LaMnO_3$ is formed by e_g states split due to the JT distortion. The splitting is somewhat underestimated in LDA+U_2. One of the reasons for this discrepancy could be an uncertainty introduced by the atomic-sphere approximation (ASA): although the ASA reproduces the insulating behavior of $LaMnO_3$ caused by the JT distortion, the split e_g bands are appreciably broadened in comparison with more precise FLAPW calculations.[7] The LDA+U_1 provides quite a reasonable description for the low energy part (up to 3 eV) of the optical spectra in the $LaMnO_3$ case as an excitation from O($2p$) to an unoccupied band formed by alternating x^2-z^2 and y^2-z^2 orbitals (around 2 eV in Fig. 3), but the next excitation in this picture appears only around 6 eV being rather far from the experimental finding.

Serious discrepancies between theoretical and experimental data were found for the $LaFeO_3$ where the low energy part of the optical conductivity curve reveals two peaks in LDA+U_2: the low intensity one around 1 eV corresponding to excitations from e_g to t_{2g} band and the higher intensity peak corresponding to transitions between occupied and unoccupied e_g bands (located at -1.0 and 2.5 eV in Fig. 3) in qualitative agreement with experimental data. Nevertheless, in the experimental curve these two peaks are almost rigidly shifted to the higher energy region by ~ 2 eV. Thus, a potential correction acting simultaneously on t_{2g} and e_g states and additionally splitting the occupied and empty states is required for this compound. This is in line with calculations of the photoemission spectra for the $LaFeO_3$,[8] where the rigid shift of the same magnitude was needed for the occupied states in order to fit experimental and theoretical (LSDA) curves. In LDA+U_1, the Fe($3d$) states with different spins are split by $U+4J \simeq 11$ eV and form very narrow bands located below and above the O($2p$) band (Fig. 3). The first excitation in this picture corresponds to a transition from the O($2p$) to the upper Fe($3d$) band separated by the charge-transfer gap ~ 1.8 eV which is in good agreement with experimental estimations. Nevertheless, the shape of the optical conductivity curve obtained in this approach is rather far from the experimental one (Fig. 5). We have also performed a series of LDA+U_1 calculations varying U as a parameter in order to find an optimal value with which the theoretical spectrum would fit the experimental one for $LaFeO_3$. Surprisingly, however, the LDA+U_1 approach, where without hybridization the correction simply has a form of rigid (constant) shift for all $3d$ states, failed to reproduce a rigid shift of t_{2g} and e_g bands on optical spectra. Actually, the strong σ-type hybridization between e_g and O($2p$) states makes the e_g band less sensitive to the strength of the on-site Coulomb interaction in comparison with the t_{2g} one.

For $LaCoO_3$ the experimental optical spectra show three peaks located around 1, 3, and 6 eV, respectively, in reasonable agreement with our finding. It is closely related with the density of occupied states for this compound (Fig. 4), which exhibits three main structures corresponding to the Co(t_{2g}) band and broad O($2p$) band split by the hybridization effects into the bonding and antibonding parts. All three structures appear in the optical conductivity curve through the excitations into the e_g band. In the LDA+U_1 approach, Co(t_{2g}) states are shifted to the bottom of the O($2p$) band by large U (Fig. 4) resulting in very poor description of the low energy part of the optical spectra.

In accordance with optical measurements,[41] $LaNiO_3$ and $LaCuO_3$ show metallic behavior, but their spectra largely deviate from the simple Drude form. Both LSDA and LDA+U_2 reproduce well experimental spectra for these compounds except the high intensity Drude peak found theoretically. For $LaCuO_3$ LDA+U_1 gives very similar results. In this compound $M(3d)$ states are "dissolved" in the O($2p$) band (Fig. 4) and optical conductivity is very insensitive to "exact" position of their center. Both for $LaNiO_3$ and $LaCuO_3$, LDA+U_1 also displays the high intensity Drude peak.

At the present stage, the origin of the high intensity peak observed in the experimental optical spectra around 10 eV is not clear. Position and intensity of this peak are almost the same for all LaMO$_3$ compounds. This peak can be hardly identified with excitations to La $4f$ states (which were not included in the valence basis in the present consideration) because absolutely the same structure has been observed for Y-based perovskites YMO$_3$.[41]

IV. SUMMARY AND CONCLUSIONS

We have applied the LDA+U approach for the transition-metal perovskites LaMO$_3$ with M=Ti–Ni assuming two different models for localization of $3d$ electrons at transition-metal sites.

(i) All $3d$ electrons are localized and experience large on-site Coulomb interaction correction.

(ii) Only $3d$ states of t_{2g} character are supposed to be localized, whereas those of e_g character, strongly interacting with $2p$ states of nearest oxygens and forming broad σ bands, are treated as itinerant in the scope of the standard LSDA approach and allowed to participate in renormalization of the on-site Coulomb interaction between t_{2g} electrons.

The first scheme predicts the insulating behavior for Ti-Co perovskites. However, regarding magnetic and optical properties, the effect of the Coulomb interaction is strongly overestimated. Moreover, the insulating behavior of $LaVO_3$ and $LaCrO_3$ in this approach corresponds to the charge-transfer rather than Mott-Hubbard picture in clear contradiction with photoemission data.

The second scheme provides more appropriate description for most of LaMO$_3$.

(i) Predicting insulating behavior for $LaTiO_3$ and $LaVO_3$ with a small (Mott-Hubbard) gap formed by the t_{2g} states. The strength of the effective Coulomb interaction between t_{2g} electrons is comparable with the t_{2g} bandwidth ($U_{\rm eff} \sim W$). This feature may be responsible for a variety of many-electron phenomena observed in these compounds.[12] Contrary to the pure LSDA picture, magnetism of $LaTiO_3$ naturally appears in this approach.

(ii) Considerably increasing the band gap of $LaCrO_3$ in comparison with the pure LSDA results and in good agreement with experimental data.

(iii) Opening a small energy band gap between t_{2g} and e_g bands in paramagnetic rhombohedral $LaCoO_3$.

(iv) Introducing almost negligible effects in the LSDA band structures for $LaMnO_3$ and $LaNiO_3$ which are charac-

terized by minimum effective Coulomb interaction parameters for t_{2g} states. This is in line with the recently proposed band (rather than strongly correlated) picture for the transition-metal perovskites[7–9] where applications of the LSDA were the most successful to explain the behaviors of the Mn- and Ni-based compounds.

The behavior of $LaFeO_3$ is still unclear. If discrepancies between theoretical and experimental data in the magnitude of the local magnetic moments can be attributed to experimental uncertainties,[7] the problem with almost rigid shift (~ 2 eV) between higher occupied and lower unoccupied states required in the band picture to reproduce experimental excitation spectra remains unsolved. A proper account of the correlation effects is needed. We believe that the band structure obtained in the LDA+U_2 approach applied to the t_{2g} states could be a good starting point for the many-body perturbation technique for the perovskite transition-metal oxides.

ACKNOWLEDGMENTS

We thank T. Arima for providing the numerical information of experimental optical spectra[41] and W.E. Pickett for sending us unpublished results[9] prior to the publication. The present work is supported partly by New Energy and Industrial Technology Development Organization (NEDO) and also partly by a Grant-in-Aid for Scientific Research in the priority area ''Anomalous Metallic States Near the Mott Transition'' from the Ministry of Education, Science and Culture of Japan.

APPENDIX A: RENORMALIZATION OF COULOMB AND EXCHANGE INTEGRALS BY e_g ELECTRONS

Let us consider the system containing two types of electrons (say d and s). We assume the following parametrization for d-type single-particle energies in terms of d and s populations (n and n_s, respectively):

$$\varepsilon^{\uparrow} = \text{const} + U^0 n^{\downarrow} + (U^0 - J^0) n^{\uparrow} + U^0_{ds} n_s \qquad \text{(A1)}$$

which corresponds to the HF approximation and is widely used to extract parameters of effective electron-electron interaction in the constrained-LSDA approach.[23,32,33] U^0 and J^0 are unrenormalized (bare) Coulomb and exchange among d electrons, U^0_{ds} is the Coulomb ds interaction parameter (we do not consider the ds exchange, thus neglecting the renormalization effects for J^0). We also neglect nonsphericity of d shell and suppose that U^0 and J^0 do not depend on orbital indices. Then, we suppose that d states themselves can be divided into two groups like t_{2g} and e_g: $n = n_{t_{2g}} + n_{e_g}$. The reason for such a separation could be an external factor like very different hybridization effects involving t_{2g} and e_g orbitals. In order to find parameters of the effective interaction for t_{2g} states ($U_{t_{2g}}$ and $J_{t_{2g}}$) we use the standard procedure and fit $\varepsilon^{\uparrow}$ to an expression given by

$$\varepsilon^{\uparrow} = \text{const} + U_{t_{2g}} n^{\downarrow}_{t_{2g}} + (U_{t_{2g}} - J_{t_{2g}}) n^{\uparrow}_{t_{2g}}. \qquad \text{(A2)}$$

Then, $U_{t_{2g}}$ and $J_{t_{2g}}$ can be found as $\delta\varepsilon^{\uparrow}/\delta n^{\downarrow}_{t_{2g}}$ and $\delta(\varepsilon^{\uparrow} - \varepsilon^{\downarrow})/\delta n^{\downarrow}_{t_{2g}}$, respectively. Using (12), $U_{t_{2g}}$ can be expressed through basic U^0, J^0, and U^0_{ds} parameters as

$$U_{t_{2g}} = U^0\left(1 + \frac{\delta n_{e_g}}{\delta n^{\downarrow}_{t_{2g}}}\right) + U^0_{ds}\frac{\delta n_s}{\delta n^{\downarrow}_{t_{2g}}} - J^0\frac{\delta n^{\uparrow}_{e_g}}{\delta n^{\downarrow}_{t_{2g}}}. \qquad \text{(A3)}$$

All fluctuations are required to obey the total charge conservation condition $n_{t_{2g}} + n_{e_g} + n_s = \text{const}$. Thus, for $U_{t_{2g}}$ we have

$$U_{t_{2g}} = U\left(1 + \frac{\delta n_{e_g}}{\delta n^{\downarrow}_{t_{2g}}}\right) - J^0\frac{\delta n^{\uparrow}_{e_g}}{\delta n^{\downarrow}_{t_{2g}}} \qquad \text{(A4)}$$

where $U = U^0 - U^0_{ds}$ is the Coulomb dd interaction screened by s electrons. The factor $1 + \delta n_{e_g}/\delta n^{\downarrow}_{t_{2g}}$ describes further renormalization of U by e_g electrons. Normally $J \sim 0.1U$ and the second term in Eq. (A4) can be dropped. Similar calculations performed for $J_{t_{2g}}$ give

$$J_{t_{2g}} = J^0\left(1 - \frac{\delta m_{e_g}}{\delta n^{\downarrow}_{t_{2g}}}\right), \qquad \text{(A5)}$$

where the spin magnetization $m_{e_g} = n^{\uparrow}_{e_g} - n^{\downarrow}_{e_g}$.

Assuming a rigid band model for charge and spin fluctuations near the paramagnetic state, $\delta m_{e_g}/\delta n_{t_{2g}} = 0$ and $\delta n_{e_g}/\delta m_{t_{2g}} = 0$. Thus, we have finally

$$U_{t_{2g}} \simeq U\left(1 + \frac{\delta n_{e_g}}{\delta n_{t_{2g}}}\right) \qquad \text{(A6)}$$

and

$$J_{t_{2g}} \simeq J^0\left(1 + \frac{\delta m_{e_g}}{\delta m_{t_{2g}}}\right). \qquad \text{(A7)}$$

*On leave from Institute of Metal Physics, Ekaterinburg, Russia. Electronic address igor@jrcat.or.jp

[1] J.G. Bednorz and K.A. Müller, Z. Phys. B **64**, 189 (1986).

[2] R. von Helmolt *et al.*, Phys. Rev. Lett. **71**, 2331 (1993); M. McCormack *et al.*, Appl. Phys. Lett. **64**, 3045 (1994); S. Jin *et al.*, Science **264**, 413 (1994); A. Urushibara *et al.*, Phys. Rev. B **51**, 14 103 (1995).

[3] R. Mahendiran *et al.*, Appl. Phys. Lett. **66**, 233 (1995).

[4] A. Asamitsu, Y. Moritomo, Y. Tomioka, T. Arima, and Y. Tokura, Nature **373**, 407 (1995).

[5] O. Gunnarsson and K. Schönhammer, Phys. Rev. Lett. **50**, 604 (1983); J. Zaanen *et al.*, *ibid.* **55**, 418 (1985); J. W. Allen *et al.*, *ibid.* **54**, 2635 (1985); F. Patthey *et al.*, *ibid.* **58**, 2810 (1987); H. Eskes and G. A. Sawatzky, *ibid.* **61**, 1415 (1988).

[6] J. Zaanen and G. A. Sawatzky, Can. J. Phys. **65**, 1262 (1987).

[7] N. Hamada, H. Sawada, and K. Terakura, in *Spectroscopy of Mott Insulators and Correlation Metals*, edited by A. Fujimori and Y. Tokura (Springer-Verlag, Berlin, 1995).

[8] D.D. Sarma, N. Shanthi, S.R. Barman, N. Hamada, H. Sawada, and K. Terakura, Phys. Rev. Lett. **75**, 1126 (1995).

[9] W.E. Pickett and D.J. Singh (unpublished).
[10] J.P. Goral and J.E. Greedan, J. Magn. Magn. Mater. **37**, 315 (1983).
[11] L. Hedin, Phys. Rev. **139**, A796 (1965).
[12] A. Fujimori, I. Hase, H. Namatame, Y. Fujishima, Y. Tokura, H. Eisaki, S. Uchida, K. Takegahara, and F.M.F. de Groot, Phys. Rev. Lett. **69**, 1796 (1992); I.H. Inoue, I. Hase, Y. Aiura, A. Fujimori, Y. Haruyama, T. Maruyama, and Y. Nishihara, *ibid.* **74**, 2539 (1995).
[13] J.P. Perdew and Y. Wang, Phys. Rev. B **33**, 8800 (1986); J.P. Perdew, *ibid.* **33**, 8822 (1986); J.P. Perdew and Y. Wang, *ibid.* **45**, 13 244 (1992).
[14] H. Sawada *et al.* (unpublished).
[15] H. Sawada, N. Hamada, and K. Terakura (unpublished).
[16] V.I. Anisimov, J. Zaanen, and O.K. Andersen, Phys. Rev. B **44**, 943 (1991).
[17] V.I. Anisimov, I.V. Solovyev, M.A. Korotin, M.T. Czyżyk, and G.A. Sawatzky, Phys. Rev. B **48**, 16 929 (1993).
[18] I.V. Solovyev, P.H. Dederichs, and V.I. Anisimov, Phys. Rev. B **50**, 16 861 (1994).
[19] C. Zener, Phys. Rev. **82**, 403 (1951); P.W. Anderson and H. Hasegawa, *ibid.* **100**, 675 (1955); P.-G. de Gennes, *ibid.* **118**, 141 (1960).
[20] M.T. Czyżyk and G.A. Sawatzky, Phys. Rev. B **49**, 14 211 (1994).
[21] F. Aryasetiawan and O. Gunnarsson, Phys. Rev. Lett. **74**, 3221 (1995).
[22] J.C. Slater, *Quantum Theory of Molecules and Solids, Vol. IV* (McGraw-Hill, New York, 1974).
[23] O. Gunnarsson, O.K. Andersen, O. Jepsen, and J. Zaanen, Phys. Rev. B **39**, 1708 (1989).
[24] J.P. Perdew and A. Zunger, Phys. Rev. B **23**, 5048 (1981).
[25] To be exact, starting from LSDA and using the arguments of Ref. 18, the total energy in LDA+U can be expressed as that of constrained LSDA plus the energy of multiplet splitting, which is partially taken into account in the single determinant approach, through the m-dependence of Coulomb and exchange parameters. Practically the latter contribution is always expected to be very small and the corresponding energy gain is not sufficient to overcome a larger positive effect associated with deviation of E_{LSDA} from the global minimum due to constraints.
[26] A.I. Liechtenstein, V.P. Antropov, and B.N. Harmon, Phys. Rev. B **49**, 10 770 (1994); B.N. Harmon, V.P. Antropov, A.I. Liechtenstein, I.V. Solovyev, and V.I. Anisimov, J. Phys. Chem. Solids **56**, 1521 (1995).
[27] O.K. Andersen, Phys. Rev. B **12**, 3060 (1975); H.L. Skriver, *The LMTO Method* (Springer, Berlin, 1984); O. Gunnarsson, O. Jepsen, and O.K. Andersen, *ibid.* **27**, 7144 (1983); O.K. Andersen, O. Jepsen, and D. Glötzel, in *Highlights in Condensed Matter Theory*, edited by F. Bassani, F. Fumi, and M.P. Tosi (North-Holland, Amsterdam, 1985), p. 59; O.K. Andersen, Z. Pawlowska, and O. Jepsen, Phys. Rev. B **34**, 5253 (1986).
[28] B. Brandow, Adv. Phys. **26**, 651 (1977).
[29] T. Mizokawa and A. Fujimori, Phys. Rev. B **51**, 12 880 (1995).
[30] J.F. Bringley *et al.*, Phys. Rev. B **47**, 15 269 (1993).
[31] D.D. Sarma and A. Chainani, J. Solid State Chem. **111**, 208 (1994).
[32] M.R. Norman and A.J. Freeman, Phys. Rev. B **33**, 8896 (1986); A.K. McMahan, R.M. Martin, and S. Satpathy, *ibid.* **38**, 6650 (1988); V.I. Anisimov and O. Gunnarsson, *ibid.* **43**, 7570 (1991).
[33] I.V. Solovyev and P.H. Dederichs, Phys. Rev. B **49**, 6736 (1994).
[34] T. Saitoh *et al.*, Phys. Rev. B **51**, 13 942 (1995).
[35] A. Chainani, M. Mathew, and D.D. Sarma, Phys. Rev. B **46**, 9976 (1992).
[36] M. Abbate *et al.*, Phys. Rev. B **47**, 16 124 (1993).
[37] Technically, the calculations of the effective interaction parameters when only some part of 3d states is supposed to be localized can be easily performed in the LMTO-ASA method. As the first step we remove the localized states from the valence basis by putting zeros into the structure constants for all matrix elements related with the localized orbitals (say of t_{2g} type) and pushing them up above the Fermi level (which is defined by all electrons except localized ones). Then, before calculating the spin density in every iteration we add in the 3d shell the number of the localized electrons required by the constraint conditions (note that the character of the localized orbitals is not important to calculate the spherically averaged spin density in ASA). Finally, the U and J can be expressed through the nonhybridized LMTO band-center potential parameters in the standard way (Refs. 23, 32, and 33).
[38] Because of considerable admixture of the $M(e_g)$ states into the O(2p) band, n_{e_g} typically differs from the e_g population prescribed by the formal valency arguments. For example, for LaMnO$_3$ case n_{e_g} is closer to 2 (half-filling), rather than 1 deduced from the ionic configuration of Mn^{3+}: $t_{2g}^3 e_g^1$.
[39] T. Moriya, Prog. Theor. Phys. **33**, 157 (1965); K. Yosida, A. Okiji, and S. Chikazumi, *ibid.* **33**, 559 (1965); P.B. Coqblin and A. Blandin, Adv. Phys. **17**, 281 (1968).
[40] K. Terakura, T. Oguchi, A.R. Williams, and J. Kübler, Phys. Rev. B **30**, 4734 (1984).
[41] T. Arima, Y. Tokura, and J.B. Torrance, Phys. Rev. B **48**, 17 006 (1993).
[42] A. Fujimori, I. Hase, Y. Tokura, M. Abbate, F.M.F. de Groot, J.C. Fuggle, H. Eisaki, and S. Uchida, Physica B **186-188**, 981 (1993); I. Hase, A. Fujimori, H. Namatame, Y. Fujishima, Y. Tokura, M. Abbate, F.M.F. de Groot, J.C. Fuggle, H. Eisaki, and S. Uchida, *ibid.* **186-188**, 1074 (1993).
[43] V.G. Bhide, D.S. Rajoria, G. Rama, and C.N.R. Rao, Phys. Rev. B **6**, 1021 (1972).
[44] V.G. Zubkov, G.V. Bazuev, V.A. Perelyaev, and G.P. Shveikin, Fiz. Tverd. Tela **15**, 1610 (1973) [Sov. Phys. Solid State **15**, 1079 (1973)].
[45] W.C. Koehler and E.O. Wollan, J. Phys. Chem. Solids **2**, 100 (1957).
[46] J.B.A.A. Elemans, B. van Laar, K.R. van der Veen, and B.O. Loopstra, J. Phys. Chem. Solids **3**, 238 (1971).
[47] A.I. Liechtenstein, M.I. Katznelson, V.P. Antropov, and V.A. Gubanov, J. Magn. Magn. Mater. **67**, 65 (1987).
[48] I.V. Solovyev, N. Hamada, and K. Terakura (unpublished).
[49] H. Sawada, N. Hamada, and K.Terakura, J. Chem. Phys. Solids (to be published); (unpublished).
[50] O. Gunnarsson, J. Phys. F **6**, 587 (1976); J.F. Janak, Phys. Rev. B **16**, 255 (1977).
[51] M.A. Korotin, G.A. Sawatzky, S. Yu. Ezhov, I.V. Solovyev, and V.I. Anisimov (unpublished).
[52] Recently, Czyżyk and Sawatzky (Ref. 20) reported their LSDA+U calculations (very similar to the LDA+U_1 scheme in our notations) for LaCuO$_3$ where they have found a stable antiferromagnetic (A-type) insulating solution with an energy gap of 0.95 eV and a local moment at Cu site of 0.98μ_B. This is different from our finding. We believe that the reason is the use of very different WS geometries in the two works: for example, the WS sphere radius for the Cu atom is 1.36 Å in the present

work and 0.92 Å in Ref. 20. It actually produces a significant difference in the basis used in the LDA+U approach for modeling the localized states. Our idea is to use orbitals which are well localized inside the WS sphere and to choose the radii in the region corresponding to the tail (rather than to the maximum) of decaying radial $3d$ wave function. In this case LDA+U results are only slightly sensitive to the shape of the basis functions beyond the central sphere (actually, reexpansion of the wave function over the other sites is defined by its weight at the WS sphere), which are different for different band-structure methods and even different LMTO representations. This ''method-independence'' of LDA+U was illustrated in Ref. 17. Moreover, our choice of WS radii is directly related to the *ab initio* scheme used in calculations of the on-site Coulomb interaction parameters (Refs. 32 and 33), where it is also assumed that the orbital is completely localized inside the WS sphere. On the contrary, in Ref. 20 the WS sphere boundary is located near the maximum of the radial $3d$ wave function and therefore the basis used to construct the on-site Coulomb corrections had an appreciable weight on the other (not Cu) sites, probably overestimating the effect of U in comparison with our results.

[53] Yu. A. Uspenski, E.G. Maksimov, S.N. Rashkeev, and I.I. Mazin, Z. Phys. B **53**, 263 (1983); M. Alouani, J.M. Koch, and M.A. Khan, J. Phys. F **16**, 473 (1986); Yu. A. Uspenski and S.V. Khalilov, Zh. Eksp. Teor. Fiz. **95**, 1022 (1989) [Sov. Phys. JETP **68**, 588 (1989)]; D. Hobbs, E. Piparo, R. Girlanda, and M. Monaca, J. Phys. Condens. Matter **7**, 2541 (1995).

[54] P.E. Blöchl, O. Jepsen, and O.K. Andersen, Phys. Rev. B **49**, 16 223 (1994).